NSRRC - J0 4995 (2015)

Morphology and Crystallization Behavior of Poly(L-lactide)/Poly(butylene oxalate) Blends

Pei-Chun Kuo, Ya-Ching Chang, Chuh-Yung Chen, Chieh-Tsung Lo

Department of Chemical Engineering, National Cheng Kung University, No. 1, University Road, Tainan City 701, Taiwan
Correspondence to: C.-T. Lo (E-mail: tsunglo@mail.ncku.edu.tw)

Received 25 July 2014; revised 12 September 2014; accepted 19 September 2014; published online 3 October 2014
DOI: 10.1002/polb.23607

ABSTRACT: The isothermal crystallization of poly(L-lactide) (PLLA) in blends with poly(butylene oxalate) (PBOX) is investigated by time-resolved small-angle X-ray scattering, differential scanning calorimetry, and optical microscopy. We focus on the temperatures at which only PLLA crystallizes while PBOX is amorphous. It is obtained that the addition of PBOX causes a reduction of the melting temperature of PLLA. The lamellar thickness of PLLA crystals decreases whereas the amorphous layer thickness increases with blend composition, suggesting the occurrence of the interlamellar incorporation upon the addition of PBOX. The crystal growth rate and morphology of PLLA/PBOX blends are analyzed by polarized optical microscopy. The spherulite growth rate of PLLA is found to increase with the addition of PBOX. Analysis of the isothermal crystallization in terms of the Lauritzen and Hoffman equation give the reduction of the fold surface free energy upon the addition of PBOX in PLLA, indicating that the mobility of the PLLA chains is significantly improved due to the presence of PBOX. © 2014 Wiley Periodicals, Inc. J. Polym. Sci., Part B: Polym. Phys. **2015**, *53*, 192–202

KEYWORDS: blends; crystal structures; crystallization

INTRODUCTION The development of biodegradable and biocompatible polymers is a crucial task because of their potential use of reducing the environmental pollution caused by plastic wastes. These biodegradable polymers are mostly derived from environmentally friendly materials, such as agriculture crops rather than the petroleum resources. Among the biodegradable polymers, poly(L-lactide) (PLLA), which can be synthesized from starch via fermentation, has been studied extensively as a promising candidate for tissue engineering, drug delivery, and packaging.[1–4] However, PLLA still cannot completely fulfill all of the application requirements due to its poor toughness and low crystallization rate.[5,6] To achieve desired properties, a strategy of blending PLLA with other biodegradable polymers, such as poly(DL-lactide) (PDLLA),[7,8] poly(D-lactide) (PDLA),[9–11] poly(butylene succinate) (PBS),[6,12] poly(ethylene succinate),[13] and poly(ε-caprolactone)[14,15] was investigated widely. Most of these blend components also originate from agricultural resources and the mass production of these polymers may cause competition between food and non-food production. Poly(butylene oxalate) (PBOX), which is derived mostly from grass, seems to be a more suitable choice to be used as a biocompatible material. Thus, blending PLLA and PBOX may generate a new material that can reduce the use of agricultural resources and provide a possibility to address the potential market demand for biodegradable materials.

The properties of semicrystalline polymer blends depend on not only the miscibility of the components, but also their crystalline structure and morphology. It is well known that the blending of one polymer component in a crystallizable polymer may affect the chain mobility, crystallization kinetics, overall crystallinity, and crystallite dimensions. From the application point of view, specific crystal morphology determines the final properties of the materials. For instance, when drug delivery is considered, crystalline regions do not degrade at the same rate as amorphous regions and blending can alter the crystalline structure and, hence, the erosion kinetics.[17] Hence a detailed understanding of the crystallization process in polymer blends is critical to the establishment of their structure property relationships.

The crystal growth rate of polymer is determined by the energy related to the transport of macromolecular chains toward the growing crystals and the energy barrier for creation of secondary nuclei.[17–19] The addition of a noncrystallizable polymer dilutes the crystallizable component at the crystal growth front, causing a depression of crystal growth rate of the crystallizable component. Chen et al. investigated the crystallization behavior of miscible blend containing PLLA and poly(4-vinylphenol) (PVPh).[20] The good miscibility between PLLA and PVPh facilitated the incorporation of PVPh molecules into the interlamellar regions, which increased the amorphous layer thickness. When PLLA was blended with its stereoisomers (PDLLA), PDLLA disturbed the PLLA diffusion to the growth sites of crystallites,

© 2014 Wiley Periodicals, Inc.

reducing the spherulite growth rate.[8] However, the lamellar thickness and amorphous layer thickness were independent of the PDLLA content, suggesting that the PDLAA molecules were excluded from both the PLLA lamellae and interlamellar regions.

However, the addition of one component with low glass transition temperature in crystallizable polymer can promote the diffusion of crystallizable molecules to the crystal growth front, leading to an increase in the crystal growth rate. For example, PBS is immiscible with PLLA, but has much lower glass transition temperature. Blends of PLLA and PBS showed a slight increase in the crystallization rate.[6] Meanwhile, PBS was expelled out of the interlamellar regions of PLLA, resulting in a reduction of the long period and amorphous layer thickness of PLLA.[12] Similarly, the addition of compatible poly(butylene succinate-*co*-L-lactide) copolymer in PLLA enhanced significantly the isothermal and nonisothermal crystallization of PLLA. The overall crystallization rate of PLLA could also be increased by the addition of PDLA.[11] This was attributed to the formation of a stereocomplex that enhanced the nucleation of PLLA crystallization. However, the crystallization mechanism and crystal structure of PLLA remained unchanged upon the addition of PDLA.[9]

In a more complicated case, when both components in a blend were able to crystallize, a complicated morphology, such as interfibrillar spherulites and interlock spherulites, was observed, which was controlled by the properties of the crystalline polymers and processing conditions.[21,22] Lai et al. investigated the crystallization behavior of miscible crystalline/crystalline blends containing PLLA and poly(ethylene glycol) (PEG).[23] The formation of PLLA crystals caused a reduction in the crystallization rate of PEG. In PLLA/poly(butylene adipate) (PBA) blends, Zhao et al. suggested that PBA formed either a crystal state or an amorphous state in the internal or external regions of the PLLA crystals, depending on the blend composition and crystallization temperature.[22] Sheth et al. investigated the miscibility and crystallization of poly(lactic acid) (PLA) and PEG.[24] PLA and PEG were miscible when the composition was <50/50. When both polymers were crystallized, the crystallization rate of PLA increased with the addition of PEG. However, the crystallinity of PEG was suppressed with the presence of PLA.

As indicated previously, PBOX can be obtained in abundance and low cost and thus, PLLA/PBOX blends seem more suitable to be used for the biocompatible materials. PBOX is a semicrystalline polymer and it crystallizes in a triclinic structure.[25] Additionally, PBOX crystallization follows regime II mechanism with the fold and lateral surface free energy of 32.37 and 17.68 mN/m, respectively. Copolymerization of PBOX with azelaic acid could decrease both the melting and glass transition temperatures of PBOX.[26] Up to date, however, studies on the crystallization of PLLA/PBOX blends are limited. In this study, we characterized the morphological evolution at the lamellae level of blends of PLLA and PBOX during isothermal crystallization at selected temperatures at which only PLLA crystallized using *in situ* small angle X-ray scattering techniques with synchrotron radiations. Further morphological information on the lamellar and amorphous layer thickness was determined using the one-dimensional correlation functions. Melting behavior and crystal growth rate were obtained by differential scanning calorimetry (DSC) and optical microscopy to form a comprehensive picture of the crystallization behavior of PLLA/PBOX blends. The knowledge of the crystal morphology of the PLLA/PBOX blends, together with their crystallization behavior and thermal properties, will help to guide the rational design of the blends for various applications.

EXPERIMENTAL

Materials

PLLA with the number-average molecular weight (M_n) of 50,400 g/mol and polydispersity index (PDI) of 1.34 was provided by Sigma-Aldrich. PBOX was synthesized following a literature method.[27,28] Briefly, 1 mol diethyl oxalate (Acros Organics) and 1.2 mol 1,4-butanediol (Alfa Aesar) were mixed in a reactor. Tetrabutyl titanate [$Ti(OBu)_4$, Sigma-Aldrich] was used as a catalyst and the mixture was kept at 140–160 °C for 4 h. After solidification and removal of alcohol, the transesterification was carried out at 180 °C for 4 h under a pressure of 1 to 3 torr to synthesize PBOX. The prepared PBOX exhibited M_n of 10,000 g/mol and PDI of 1.90. A series of blends varying composition was prepared by dissolving known quantities of PLLA and PBOX in chloroform (1% w/w). The blends were dried slowly in air and stored in a desiccator.

Differential Scanning Calorimetry

The thermal properties of PLLA and its blends with PBOX were measured using a Perkin Elmer DSC 7 instrument. The thermal response of the instrument was calibrated with indium standards. Isothermal melt-crystallization was carried out in the temperature range of 110–125 °C. Weighted samples (~5 mg) encapsulated in aluminum pans were initially heated to 200 °C at a rate of 20 °C/min and held at the temperature for 10 min to erase the previous thermal history. The samples were then rapidly quenched to a desired crystallization temperature and maintained isothermally until the crystallization was completed. After quenching to −30 °C, the samples were reheated to above their corresponding melting temperatures at a heating rate of 10 °C/min. The glass transition temperature was determined as the midpoint of the heat capacity increment associated with the glass-to-rubber transition. The melting temperature was taken as the maximum peak value of the endothermal phenomena in the DSC curve.

Small Angle-X-Ray Scattering (SAXS)

Samples for SAXS measurement were prepared via melting blends into DSC aluminum sample pans (Perkin Elmer). The sample thickness was 1 mm. The sample pans made ideal sample holders because the aluminum was fairly transparent to the high-brilliance X-rays, and the rigid pans maintained the sample thickness when polymers were melted in the

vertically mounted SAXS sample chamber.[16] The SAXS measurements were performed at the Sector 23A1 at the National Synchrotron Radiation Research Center in Taiwan. During SAXS measurements, samples were heated with a cartridge heater at temperatures above the melting temperatures of two species for at least 10 min to eliminate any crystallization. Samples were rapidly quenched to a crystallization temperature to allow for crystallization. The sample to detector distance was 2 m and the X-ray energy was 8 keV. Data were collected at 10-s intervals during isothermal crystallization over the range of the scattering vector (q) from 0.005 to 0.21 $Å^{-1}$, where $q = 4\pi\sin(\theta/2)/\lambda$, θ is the scattering angle, and λ is the incident radiation wavelength. The scattering data were appropriately corrected for incident flux, absorption, detector sensitivity variation, and dark current, and the scattering intensity was azimuthally averaged to obtain the one-dimensional intensity data [$I(q)$] as a function of q.

Polarized Optical Microscopy

The nucleation behavior and crystalline morphology of neat PLLA and its blends with PBOX were analyzed by polarized optical microscopy. The blends of PLLA and PBOX in 1% w/w chloroform solution were cast on glass cover slips at room temperature. After allowing the solvent to evaporate slowly in air, the specimens were dried under vacuum for a day to remove all traces of solvent. After drying, the polymer films were covered by a second cover slip at 190 °C to form a specimen with a thickness of ~20 μm. Optical microscopy was carried out with a Nikon H550L Eclipse 50i LV-UEPI microscope in conjunction with a hot stage. The polymer films were rapidly heated to 200 °C where it was held for 10 min. The samples were then quenched to selected crystallization temperatures. The subsequent growth of crystalline species after quenching was recorded using a Sony color video camera (SSC-DC80 Super Exwave). The growth rate G ($= dR/dt$, where R is the radius of spherulites) was determined by measuring the radius of the spherulites as a function of time during the isothermal crystallization process. Reported spherulitic growth rates were determined as the mean of the rates from at least 20 spherulites, monitored on from several samples.

SAXS Analysis

The SAXS data were analyzed using the one-dimensional correlation function [$\gamma(r)$]. The one-dimensional correlation function, which offers more details of the microstructure, is the Fourier transform of the Lorentz-corrected SAXS profile.[29]

$$\gamma(r) = \frac{1}{Q}\int_0^\infty q^2 I(q)\cos(qr)dq \quad (1)$$

where Q is the scattering invariant. Since the SAXS data are collected in a limited angular range, they must necessarily be extrapolated to both high and low q values before Fourier transform.[30] The extrapolation to high q was performed with the aid of Porod's law, given by[31]

$$I(q) = \frac{K_p}{q^4}\exp(-\sigma_1^2 q^2) + I_b \quad (2)$$

Here, I_b is the contribution to scattering from local electron density fluctuations in the amorphous phase, K_p is a Porod law constant, and σ_1 is the transition thickness between crystalline and amorphous phases. However, extrapolation to q = zero in the region of the beam stop was accomplished by the extrapolation of the intensity using Debye-Bueche approximation[32]

$$I(q) = \frac{I(0)}{(1+q^2\xi^2)^2} \quad (3)$$

where ξ is the correlation length.

The scattering invariant is related to the morphological parameters as summarized in eq 4.[29]

$$Q = \int_0^\infty q^2 I(q)dq = W_c(1-W_c)(\eta_c - \eta_a)^2 \quad (4)$$

Here, W_c and η_c are the linear degree of crystallinity and electron density in the crystalline phase and η_a is the electron density in the amorphous phase. By the assumption of the two-phase model proposed by Strobl and Schneider,[29] the average long period (L) can be obtained from the first maximum of the correlation curve. However, the linear degree of crystallinity within the lamellar stacks can be determined by the following equation

$$\gamma_0/L = W_c(1-W_c) \quad (5)$$

where γ_0 is the ordinate corresponding to the first zero of the abscissa in the correlation function. It has to be pointed out that eq 5 is restricted to the condition that $W_c > 0.5$. If $W_c < 0.5$, W_c is replaced by $(1 - W_c)$ in the above expression. The obtained linear degree of crystallinity using eq 5 can further be used to determine the average lamellar thickness (l_c), which is the product of the long period and the linear degree of crystallinity. The difference between the long period and the lamellar thickness gives the average amorphous layer thickness (l_a).

RESULTS AND DISCUSSION

Thermal Behavior

Figure 1 shows the DSC scans of neat PLLA and its blends with PBOX after isothermal crystallization at 110 °C. A small exothermal phenomenon prior to the endothermal melting was observed. This behavior was associated to the fast crystallization rate at low crystallization temperature. When the crystallization rate is much faster than the time required for chain disentanglement, the restricted chain mobility reduced both the degree of perfection of the crystals and the maximum crystallinity, preventing the growth of well developed lamellar crystals.[1] Similar behavior was observed for PLLA[1] and other thermoplastic polymers such as poly(thio-1,4-phenylene)[33,34] and poly(aryl ether ether ketone).[35] The degree of crystallinity, calculated using 135 J/g as the

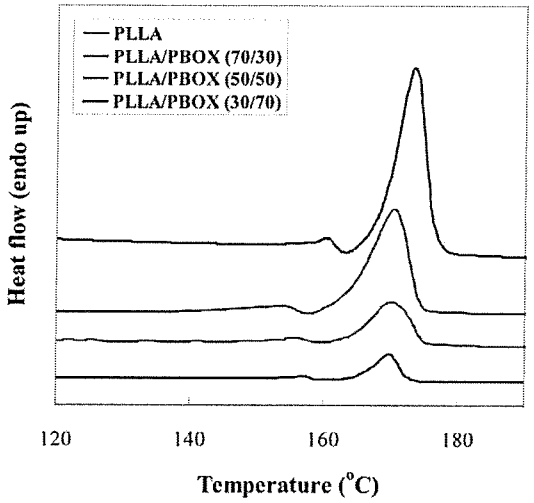

FIGURE 1 DSC melting endotherms of neat PLLA and its blends with PBOX after isothermal crystallization at 110 °C. [Color figure can be viewed in the online issue, which is available at wileyonlinelibrary.com.]

enthalpy of fusion of PLLA crystals having infinite crystal thickness,[2] was 0.35, 0.22, 0.16, and 0.10 for the neat PLLA and the blends containing 30, 50, and 70 wt % PBOX, respectively.

Figure 2 summarizes the variation of the obtained melting points of neat PLLA and its blends as a function of crystallization temperature (T_c). In comparison of the melting point of neat PLLA and its blends with PBOX, the melting behavior in PLLA/PBOX was affected considerably, showing a reduction of the PLLA melting point with an increase in PBOX content. The depression of the melting point with the addition of PBOX suggested that PLLA and PBOX are miscible. To obtain the equilibrium melting temperature (T_m^o) of PLLA and its blends, the linear Hoffman-Weeks extrapolative method was carried out.[36] Based on this method, the intersection of a least-squared line, fit to each $T_m - T_c$ data set, with the line $T_m = T_c$ gives the values of T_m^o as demonstrated in Figure 2. The obtained T_m^o shows a gradual depression from 199.2 °C for neat PLLA to 191.8, 189.9, and 189.0 °C for the blends containing 30, 50, and 70 wt % PBOX, respectively. This decreasing equilibrium melting temperature of PLLA upon the addition of the second component is attributed to the thermodynamics consideration that the chemical potential of a polymer decreased by the addition of a miscible diluent.[37] This behavior is in good agreement with other reported experimental results on the blends containing PLLA and the other miscible or partially miscible component.[38,39] However, further addition of PBOX only resulted in a slight incremental decrease of the equilibrium melting point, suggesting a relatively low miscibility between PLLA and PBOX.

Figure 3 shows the glass transition temperature (T_g) of PLLA and its blends characterized by DSC. The DSC profile of the neat PLLA exhibited a single transition and the T_g value was 60.0 °C. By contrast, the PLLA/PBOX blends showed two transitions with a higher T_g value of 47.7, 42.7, and 37.8 °C for the blends containing 30, 50, and 70 wt % PBOX, respectively. The higher T_g was associated to the chain mobility of PLLA. The depression of the higher T_g value with increasing PBOX content indicated that the addition of PBOX facilitated the chain mobility of PLLA. However, a lower T_g occurred at the temperature below 20 °C was originated from the chain mobility of PBOX. The lower T_g value increased slightly when the PLLA content increased. The appearance of two transitions in the blends located at the temperatures between those of the individual components was the evidence that PLLA and PBOX were phase separated. However, the varied T_g values with the blend composition suggested that PLLA and PBOX were partially miscible.

Crystalline Lamellar Characteristics

For each sample crystallized at selected temperatures, the raw I versus q data were converted to Lorentz-corrected intensities and the one-dimensional correlation functions were generated. Figure 4 illustrates the typical time-resolved SAXS profiles of neat PLLA and its blends with PBOX crystallized at 120 °C. For all the experiments conducted on these polymers, some residual crystallinity appeared at the beginning of the experiment, as evidenced by the presence of a weak peak at time = 0 in the intensity data, despite the annealing during the sample preparation. This was attributed to crystals nucleating during quenching the sample to the crystallization temperature. With increasing time, it is seen that the scattering peak developed and increased to a plateau value at long time. The lack of the higher order reflections of the primary peaks is primarily due to the polydispersity in the lamellar stack thickness.[40–42]

Figure 5 presents the one-dimensional correlation functions and Figure 6 shows the corresponding lamellar variables for

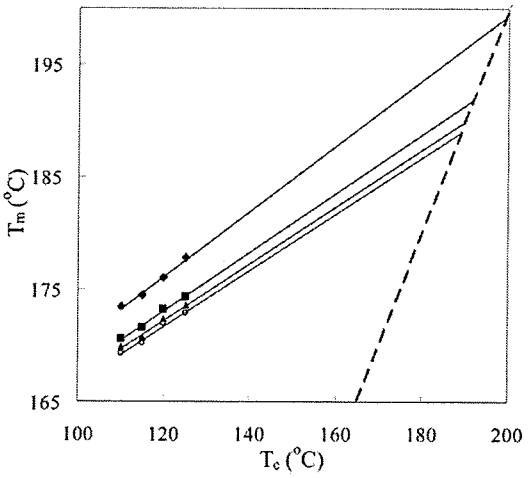

FIGURE 2 Variation of the melting points for neat PLLA and its blends with PBOX as a function of crystallization temperature. The solid line represents the relationship between the observed $T_m - T_c$ data according to the linear Hoffman-Weeks extrapolative method. (◆) 100:0 PLLA/PBOX, (■) 70:30 PLLA/PBOX, (▲) 50:50 PLLA/PBOX, and (○) 30:70 PLLA/PBOX.

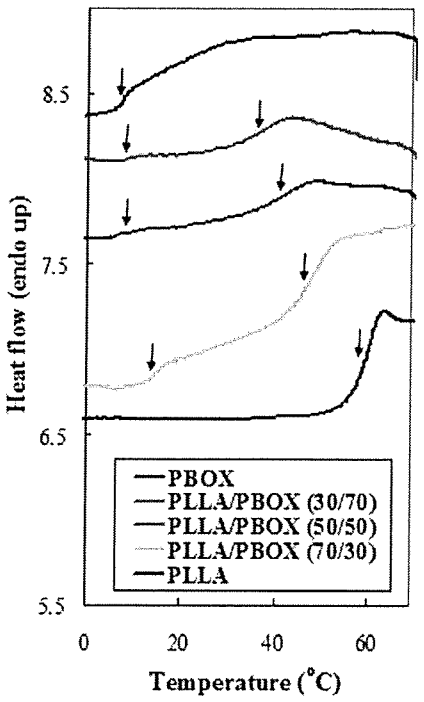

FIGURE 3 DSC thermograms of melt-quenched neat PLLA and its blends with PBOX. The arrows show T_g value. [Color figure can be viewed in the online issue, which is available at wileyonlinelibrary.com.]

the various blends isothermally crystallized at 120 °C. As mentioned in the previous section, there are two possible solutions for the degree of crystallinity and it is not possible to mathematically distinguish between them. Our rational for using the smaller solution for the degree of crystallinity to calculate the lamellar thickness was based on the low bulk degree of crystallinity obtained from DSC.

In Figure 6(a), there is an induction time and at this time, the signal intensity is not sufficient for evaluation of the lamellar parameters for the neat PLLA. For longer times, the change in the long period is not significant and is about independent of time within the experimental error. A similar trend is seen for the various blends crystallized at the selected temperature. However, the lamellar thickness for neat PLLA and PLLA/PBOX blends progressively increased with time, reaching nearly a constant value at longer times, meaning that thicker crystalline layers formed during isothermal crystallization. Meanwhile, the average amorphous layer thickness was found to decrease at early crystallization times for all the PLLA and PLLA/PBOX blends and then remain constant throughout the duration of crystallization. The decrease of the average amorphous layer thickness was considerably for the neat PLLA and the blend with the small amount of PBOX. As crystallization proceeded, the crystallizable chains in the amorphous region migrated toward the lamellar crystals and participated in the crystallization process. This migration reduced the amorphous layer thickness. The increase in the lamellar thickness could be related to the lamellar thickening. When the large amount of PBOX was added in the blends, some PBOX chains were trapped in the amorphous region inside the PLLA lamella stacks, which caused the increase of the amorphous layer thickness and the decrease of the lamellar thickness. The trapped PBOX chains and the migrated PLLA chains toward the lamellar crystals had the opposite effect on the change in the morphological parameters. As a result, the variations of both the lamellar thickness and the amorphous layer thickness in the blends with the higher PBOX content were not significant when compared to those in the blends with the lower PBOX content.

The variation of the morphological parameters of PLLA and PLLA/PBOX isothermally crystallized for a long period of time is summarized in Figure 7. Both L and l_c values were seen to increase with crystallization temperature especially in the low PBOX content. Additionally, the addition of PBOX in PLLA reduced the l_c values. This result was in good agreement with the depression of the melting point of PLLA crystalline in the PLLA/PBOX blends. However, the amorphous layer thickness increased with blend composition, suggesting the occurrence of the interlamellar incorporation upon the addition of PBOX. As the PBOX composition is high, the nearly constant value of l_a implies that the additional PBOX molecules were expelled out of the interlamellar regions and consequently were trapped in the interfibrillar and interspherulitic regions.

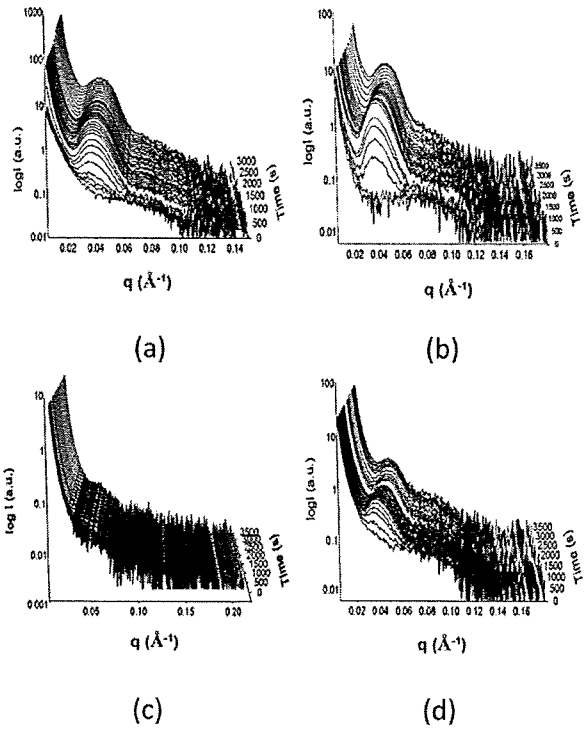

FIGURE 4 Time-resolved SAXS profiles obtained during isothermal crystallization at 120 °C. (a) PLLA; (b) 70:30 PLLA/PBOX; (c) 50:50 PLLA/PBOX; and (d) 30:70 PLLA/PBOX.

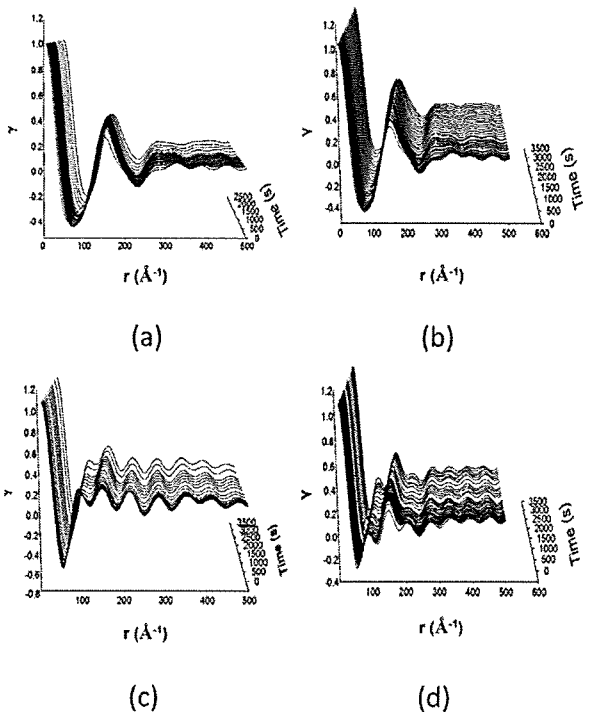

FIGURE 5 $\gamma(r)$ profiles of neat PLLA and its blends with PBOX crystallized at 120 °C. (a) PLLA; (b) 70:30 PLLA/PBOX; (c) 50:50 PLLA/PBOX; and (d) 30:70 PLLA/PBOX.

Spherulite Growth

Figure 8 shows the crystal morphology of neat PLLA and its blends with PBOX crystallized at 110 °C. When crystallized from the melt, PLLA and its blends with PBOX grew spherulites, which exhibited the characteristic Maltese cross pattern under the polarized microscope. The Maltese cross pattern was caused by the different light refractivity between crystalline and amorphous phases. Spherulites grown in blends additionally exhibited banding with radial separations in the range of 10–20 μm.

Such banding is typical in polymer spherulites and is caused by a twisting of crystallographic orientation about radii that reflects cooperative twisting of radiating lamellar crystals about their axes of fastest growth.[43] Its occurrence implies a high degree of coordination in packing of lamellae within fairly compact structures. For neat PLLA, Wang and Mano[44] reported a banding to nonbanding morphological transition of PLLA spherulites occurring at 135–140 °C. This agrees well with the nonbanded spherulites of PLLA in our work since it crystallized at much lower temperature. Meanwhile, the onset temperature of banded spherulites was shifted to lower crystallization temperature by the presence of a diluent.[45] Keith et al. reported that the banding feature in blends is much more regular and exhibited smaller spacings.[43] In our work on blends of PLLA and PBOX, only a moderate influence on the structure of the banded spherulites is observed with increasing blend composition.

The most notable effect of spherulite growth upon the addition of PBOX is the remarkable potency in reducing nucleation of spherulites. This suggested that the blending of PBOX in PLLA diluted nucleation sites and raised the energy barrier for the nucleation of PLLA crystals. Figure 9 shows the change in the radius of spherulites with time for various blend compositions prior to the spherulite impingement. In neat PLLA and its blends with PBOX, the radii of the spherulites increased linearly with time before the occurrence of spherulite impingement. After impingement, the spherulites continued to fill the rest of the available space and the growth of these spherulites would be prohibited at the boundaries between impinged spherulites. This naturally slowed the rate of crystallization.

The spherulite growth rate of PLLA crystalline was calculated via the slope of the regression line fitted to the experimental data at a given crystallization temperature. Figure 10 shows the average spherulite growth rate of PLLA and its blends with PBOX crystallized at different temperatures. In comparison of the spherulite growth rate of the blends, the incorporation of PBOX promoted the growth of spherulites. It is well known that the spherulite growth rate of polymers depends on the parameters that characterizing the system, including the blend composition, molecular weight, crystallization temperature, and glass transition temperature. Since there are complex parameters that affect the spherulite growth rate, the addition of amorphous polymer may cause either a depression or an increase in the spherulite growth rate of the crystallizable component. In a situation that the glass transition temperature of the amorphous diluent is lower than that of the crystallizable component as such in our case, the mobility of the molecules of the crystallizable component in the blend is higher than that in its homopolymer melt. The addition of the amorphous diluent would facilitate both the motion of the crystallizable component in the melt towards the growing crystals and the arrangement of the chains into the crystals, giving a positive contribution to the spherulite growth rate. Such behavior was also observed in PLLA blended with polyethylene oxide[46] and triphenyl phosphate.[47]

The kinetic data obtained from Figure 10 have been examined in terms of the Lauritzen and Hoffman theory.[48] The general expression for the growth rate of a linear polymer crystal with folded chains is given by

$$G=G_0\exp\left(\frac{-U^*}{R(T_c-T_\infty)}\right)\exp\left(-\frac{K_g}{T_c\Delta Tf}\right) \quad (6)$$

Here, G_0 is the pre-exponential factor, K_g is the nucleation constant, U^* is the activation energy for segment diffusion to the site of crystallization, $\Delta T = T_m^\circ - T_c$ is the degree of supercooling, T_∞ is the hypothetical temperature where all motion associated with viscous flow ceases ($= T_g - 30$ K), $f = 2T_c/(T_m^\circ + T_c)$ is the correction factor, and R is the gas constant. The first exponential term in eq 6, $\exp[-U^*/R(T_c - T_\infty)]$, indicates the chain transport effect on the

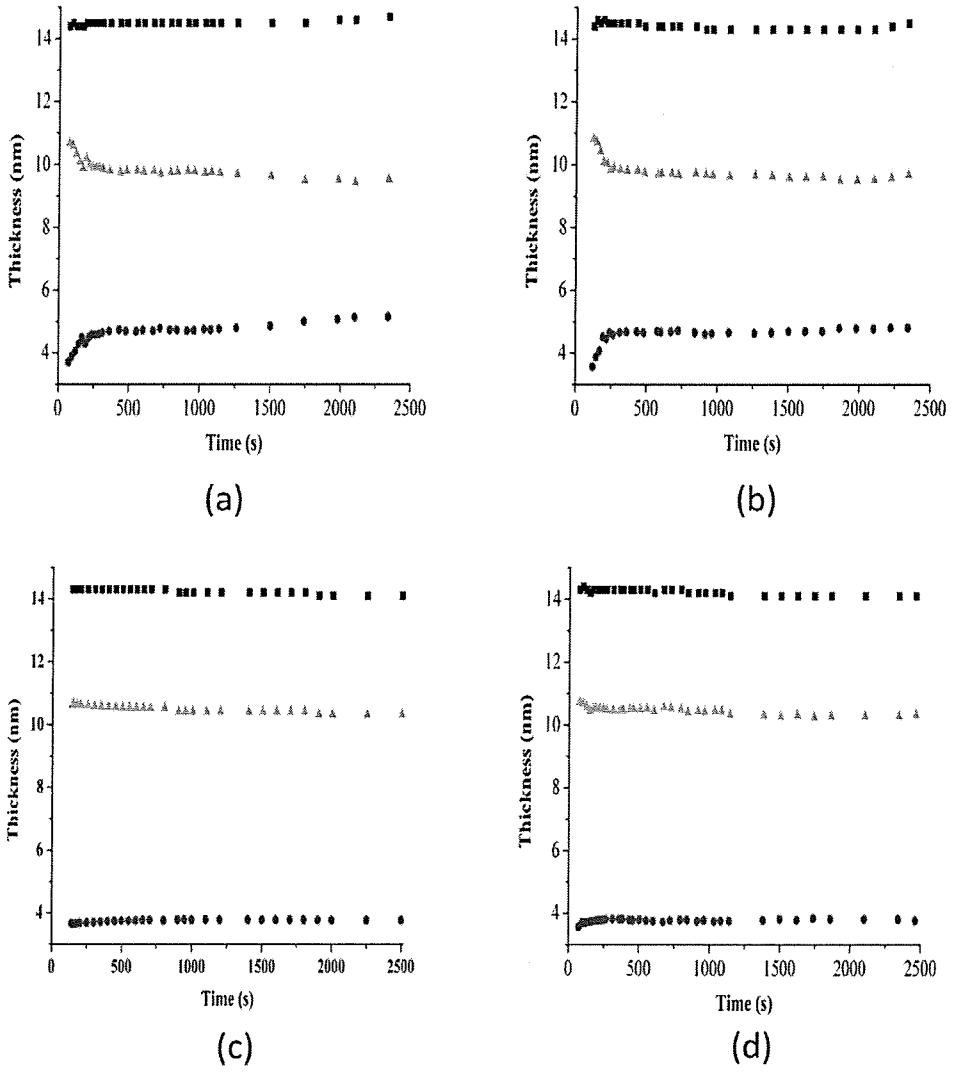

FIGURE 6 The morphological parameters of neat PLLA and its blends with PBOX crystallized at 120 °C obtained from SAXS. (a) PLLA; (b) 70:30 PLLA/PBOX; (c) 50:50 PLLA/PBOX; and (d) 30:70 PLLA/PBOX. (■) L, (▲) l_a, and (●) l_c. [Color figure can be viewed in the online issue, which is available at wileyonlinelibrary.com.]

interface. The second term, $\exp(-K_g/T_c\Delta Tf)$, represents the secondary nucleation effect. Table 1 lists the Lauritzen and Hoffman parameters used for the nucleation analysis and Figure 11 shows the plot of $[\ln(G) + U^*/R(T_c - T_\infty)]$ versus $[1/(T_c\Delta Tf)]$, which gives the values of K_g and G_0 from their slopes and intercepts, respectively. The nucleation parameter, K_g is given by

$$K_g = \frac{nb_o\sigma\sigma_e T_m{}^o}{\Delta H_f k_B} \tag{7}$$

Here, b_o is the crystal layer thickness, σ is the lateral surface free energy, σ_e is the fold surface free energy, ΔH_f is the heat of fusion per unit volume, and k_B is the Boltzmann constant. The constant n is 4 for regimes I and III and 2 for regime II. Because the determination of the surface free energy product ($\sigma\sigma_e$) in eq 7 is complicated by an uncertainty of the crystallization regime, we used the Lauritzen Z-test in eq 8 to distinguish between regimes I and II, but regime III is not considered in this approach.[48]

$$Z \approx 10^3\left(\frac{L_0}{2a_0}\right)^2 \exp\left[(-X/(T_c\Delta T))\right] \tag{8}$$

where L_0 is the effective lamellae width and a_0 is the lattice constant. If $X = K_g$ yields $Z \leq 0.01$, crystallization follows regime I. On the contrary, if $X = 2K_g$ leads to $Z \geq 1$, the regime II kinetics is obeyed. As pointed out by Lauritzen and Hoffman[48] and Wang and Nishi,[50] it is more convenient to use the known values of K_g and the inequalities for the Z value to obtain the value of L_0 in the two regimes and then further to justify the realistic of such values. Application of

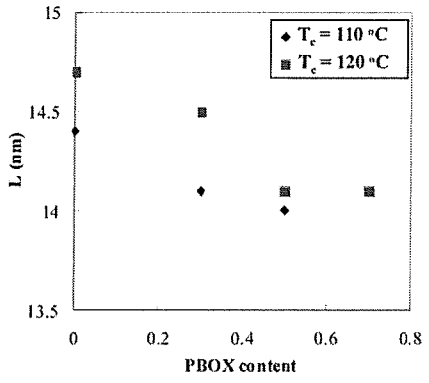

(a)

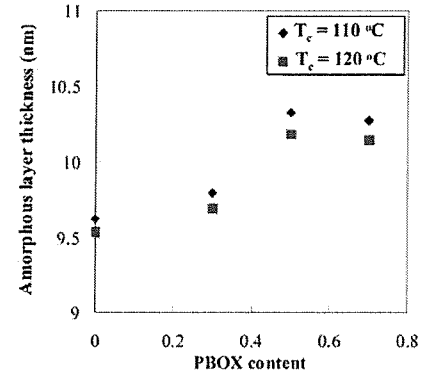

(b)

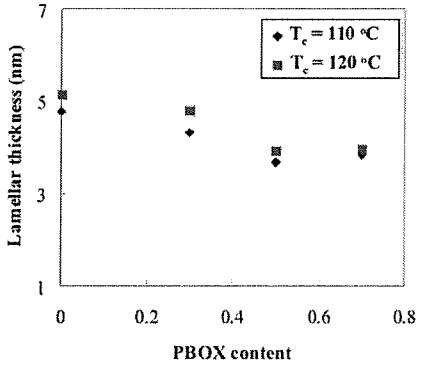

(c)

FIGURE 7 Composition variations of morphological parameters of the neat PLLA and its blends with PBOX. (a) L; (b) l_a; and (c) l_c. [Color figure can be viewed in the online issue, which is available at wileyonlinelibrary.com.]

the Z test to the PLLA in the entire range of T_c leads to the following results. If crystallization occurs in regime I, L_0 cannot be more than 123 nm. In contrast, if the crystallization is assumed to be in regime II, L_0 is $>2.5 \times 10^{-8}$ nm. Both values seem to be realistic and it is not possible to determine the crystal regime by simply applying the Lauritzen Z-test.

Previous work reported the PLLA crystallization with a transition from regime II to regime III at a temperature of around 120 °C and the crystallization mechanism below 120 °C belongs to regime III.[51–54] Based on the published work, regime III mechanism was assigned in our work to calculate the growth rate parameters and the results are shown in Table 2. The suppression of K_g with increasing PBOX content implied lower surface free energy of the lamellar crystals, which is associated to the compatibility effect.

According to the published σ value of 12.03 mN/m,[49] the value of the fold surface free energy was estimated and the σ_e value for all the blends investigated are also summarized in Table 2. The σ_e value of neat PLLA obtained in this work is 76.2 mN/m, which is in the range of 63–107 mN/m listed in a literature.[2] The σ_e value of blends ranged between 57.6 and 69.9 mN/m, with the values for the blends smaller than that of the neat PLLA, indicating that the presence of PBOX decreased the fold surface free energy of the blends. As σ_e is correlated with the work of chain folding, the lower σ_e value in blends suggested that the mobility of the PLLA chains in the interspherulitic regions is significantly improved due to the presence of PBOX.

In contrast to the secondary nucleation theory, Strobl proposed a multistage model to describe the crystallization process.[55,56] This model suggested that a mesomorphic layer formed at the growth front between the lateral crystal face and the melt. Hence, polymer crystallization and melting are controlled by T_m° and a characteristic temperature, T_c^∞. The melting temperature of a crystal with a thickness l_c was correlated by the Gibbs-Thomson equation.[57] This equation describes the reduction of the melting temperature below the equilibrium value of a macroscopic body caused by the excess fold surface free energy. The obtained T_m° values of the PLLA and its blends according to the Gibbs-Thomson equation were 206.0, 196.3, 195.2, and 194.3 °C for PLLA and the blends containing 30, 50, and 70 wt % PBOX, respectively. The T_m° values were slightly larger than those obtained by the Hoffman-Weeks expression and exhibited composition dependence. However, an empirical relationship between T_c^∞ and l_c was obtained by the modified Gibbs-Thomson equation, described by[56]

$$\frac{1}{l_c} = C_c(T_c^\infty - T_c) \tag{9}$$

According to this expression, the T_c^∞ values of the PLLA and its blends were 241.3.0, 214.1, 212.4, and 211.1 °C for PLLA and the blends containing 30, 50, and 70 wt % PBOX, respectively. The T_c^∞ values were 15–35 °C higher than the T_m° values, which were consistent with the difference between the two values for other polymers, such as 10 °C for polyethylene, 30 °C for poly(ε-caprolactone), and 20 °C

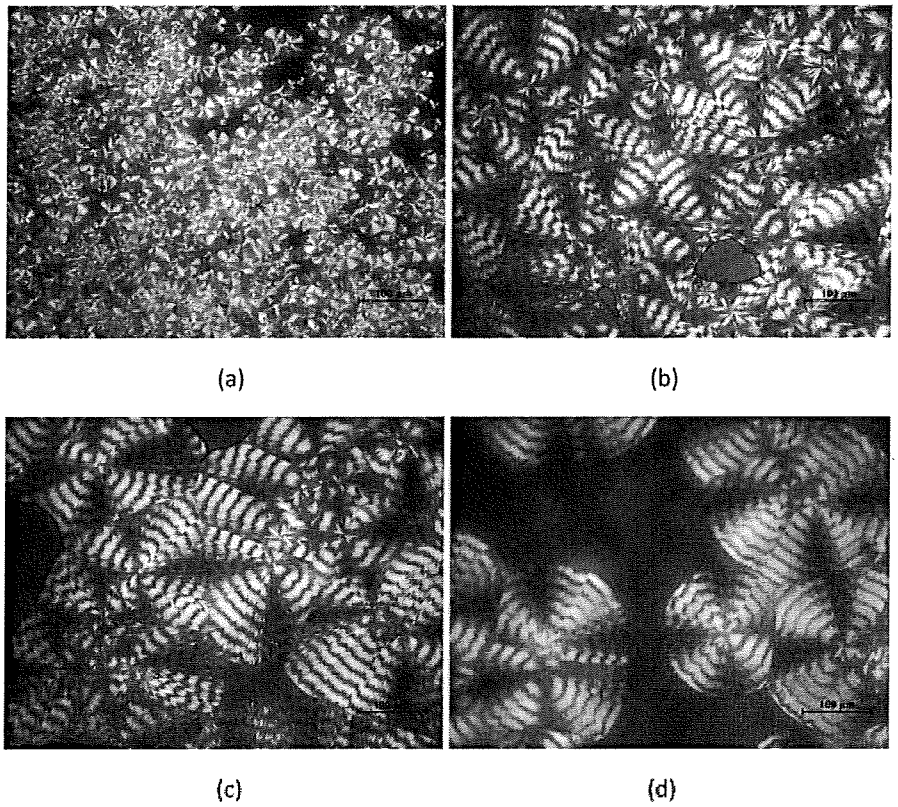

FIGURE 8 Spherulite growth of neat PLLA and its blends with PBOX crystallized at 110 °C. (a) PLLA; (b) 70:30 PLLA/PBOX; (c) 50:50 PLLA/PBOX; and (d) 30:70 PLLA/PBOX. [Color figure can be viewed in the online issue, which is available at wileyonlinelibrary.com.]

for isotactic polystyrene.[55] In addition to these transition temperatures, Strobl further suggested the correction of the expression of the spherulite growth rate via using a zero-growth temperature rather than T_m^o. In our study, we still used the classical Lauritzen and Hoffman theory to analyze polymer crystallization because we did not have reasonable data to prove the mesomorphic state of PLLA and its blends with PBOX. However, by using the secondary nucleation

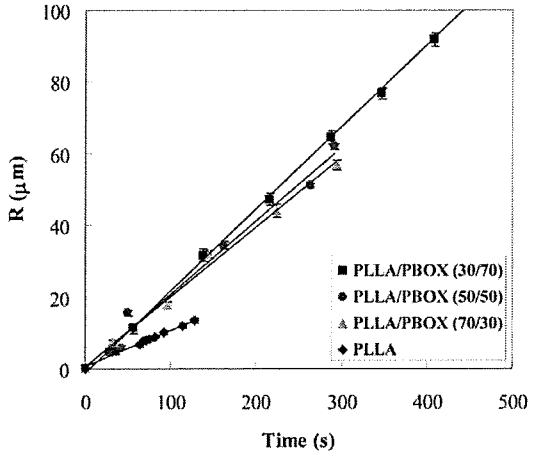

FIGURE 9 The radius of the spherulites of neat PLLA and its blends with PBOX as a function of time. The crystallization temperature is 110 °C. [Color figure can be viewed in the online issue, which is available at wileyonlinelibrary.com.]

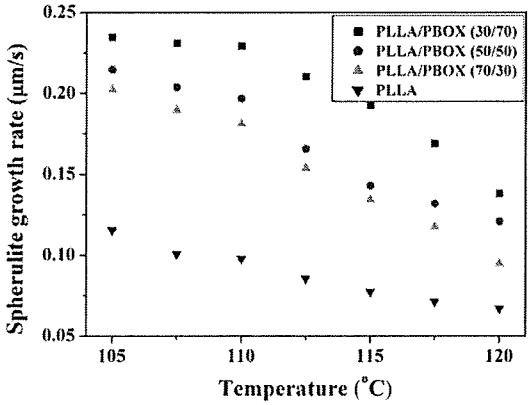

FIGURE 10 The spherulite growth rate of neat PLLA and its blends with PBOX as a function of crystallization temperature. [Color figure can be viewed in the online issue, which is available at wileyonlinelibrary.com.]

TABLE 1 Lauritzen and Hoffman Parameters used for the Nucleation Analysis[49]

Parameter	Value
U^*	1500 (cal/mol)
T_g	333.5 (K)
ΔH_f	1.11×10^8 (J/m^3)
b_0	0.517 (nm)
a_0	0.597 (nm)
σ	12.03 (mN/m)

theory, the effect of PBOX on the PLLA crystallization was obtained, which is the main focus of this study.

CONCLUSIONS

A systematic study of the crystal growth and morphology of PLLA/PBOX blends has been performed over a wide range of compositions and crystallization temperatures. The results on the glass transition temperature suggested that PLLA is partially miscible with PBOX across the entire range of compositions. A kinetic analysis of morphological details at the lamellar level using *in situ* SAXS showed a progressive increase in the lamellar thickness for both neat PLLA and PLLA/PBOX blends with time, following a plateau at longer times, suggesting that thicker crystalline layers formed during isothermal crystallization. However, for the blends containing larger amount of PBOX, the change in the morphological parameters was less pronounced. This was attributed to the PBOX chains that trapped in the amorphous region inside the PLLA lamella stacks, which caused the increase of the amorphous layer thickness and the decrease of the lamellar thickness. The effect of the trapped PBOX on the change of the morphological parameters was opposite to the crystal thickening effect during crystallization. As a result, the variations of both the average lamellar thickness and the amorphous layer thickness in the blends with the higher PBOX content were not significant. After complete crystallization, the amorphous layer thickness increased with blend composition. This behavior also suggested the occurrence of the interlamellar incorporation upon the addition of PBOX.

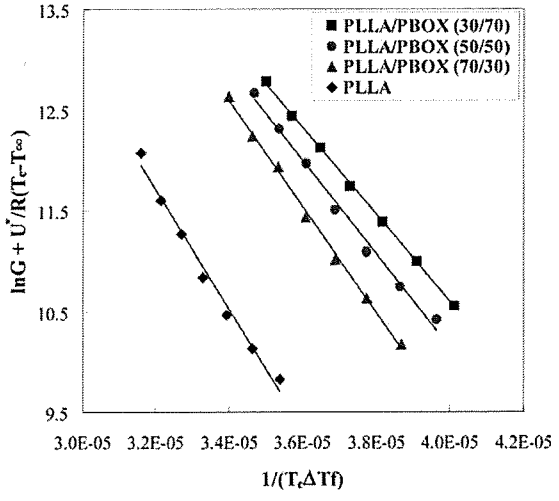

FIGURE 11 The Plot of $[\ln G + U^*/R(T_c - T_\infty)]$ versus $[1/T_c\Delta Tf]$ for neat PLLA and its blends with PBOX. [Color figure can be viewed in the online issue, which is available at wileyonlinelibrary.com.]

TABLE 2 The Growth Rate Parameters for PLLA and Its Blends with PBOX

Polymer	$K_g \times 10^{-5}$ (K^2)	$\sigma\sigma_e \times 10^6$ (N^2/m^2)	σ_e (mN/m)
PLLA	5.84	916.1	76.2
70:30 PLLA/PBOX	5.28	841.4	69.9
50:50 PLLA/PBOX	4.58	732.9	60.9
30:70 PLLA/PBOX	4.32	692.3	57.6

With regard to the morphological observations using polarized optical microscopy, the neat PLLA crystallized in a spherulitic form, and the spherulites grew to a banded structure upon the addition of PBOX. Meanwhile, the spherulite growth rate showed clear composition dependence, having the larger spherulite growth rate with increasing PBOX content. This is due to the addition of the amorphous diluent with lower glass transition temperature that facilitated both the motion of the crystallizable component in the melt towards the growing crystals and the arrangement of the chains into the crystals, giving a positive contribution to the spherulite growth rate. Analysis of the isothermal crystallization in terms of the Lauritzen and Hoffman equation indicated that the introduction of PBOX in PLLA reduced the fold surface free energy. This result is consistent with our DSC thermograms that the mobility of the PLLA chains was significantly improved due to the presence of PBOX.

ACKNOWLEDGMENTS

This work is financially supported by National Science Council in Taiwan under Grant No. NSC 100-2628-E-006-001 and the Technology Development Program for Academia No. 101-EC-17-A-08-S1-204 by Ministry of Economic Affairs in Taiwan.

REFERENCES AND NOTES

1 S. Iannace, L. Nicolais, *J. Appl. Polym. Sci.* **1997**, *64*, 911–919.

2 T. Miyata, T. Masuko, *Polymer* **1998**, *39*, 5515–5521.

3 Z. H. Zhou, J. M. Ruan, Z. C. Zhou, J. P. Zou, *Polym.-Plast. Technol. Eng.* **2007**, *46*, 863–871.

4 P. Badrinarayanan, K. B. Dowdy, M. R. Kessler, *Polymer* **2010**, *51*, 4611–4618.

5 H. Urayama, T. Kanamori, K. Fukushima, Y. Kimura, *Polymer* **2003**, *44*, 5635–5641.

6 M. Shibata, Y. Inoue, M. Miyoshi, *Polymer* **2006**, *47*, 3557–3564.

7 J. Xu, B. H. Guo, J. J. Zhou, L. Li, J. Wu, M. Kowalczuk, *Polymer* **2005**, *46*, 9176–9185.

8 L. Bouapao, H. Tsuji, K. Tashiro, J. Zhang, M. Hanesaka, *Polymer* **2009**, *50*, 4007–4017.

9 L. Bouapao, H. Tsuji, *Macromol. Chem. Phys.* **2009**, *210*, 993–1002.

10 H. Tsuji, K. Tashiro, L. Bouapao, M. Hanesaka, *M. Polymer* **2012**, *53*, 747–754.

11 Y. Li, C. Han, *Ind. Eng. Chem. Res.* **2012**, *51*, 15927–15935.

12 J. W. Park, S. S. Im, *J. Appl. Polym. Sci.* **2002**, *86*, 647–655.

13 J. Lu, Z. Qiu, W. Yang, *Polymer* **2007**, *48*, 4196–4204.

14 D. W. Grijpma, R. D. A. Van Hofslot, H. Super, A. J. Nijenhuis, A. Pennings, *Polym. Eng. Sci.* **1994**, *34*, 1674–1684.

15 M. Hiljanen-Vainio, P. Varpomaa, J. Seppla, P. Tormala, *Macromol. Chem. Phys.* **1996**, *197*, 1503–1523.

16 M. J. Kipper, S. Seifert, P. Thiyagarajan, B. Narasimhan, *J. Polym. Sci. Part B: Polym. Phys.* **2005**, *43*, 463–477.

17 J. D. Hoffman, *SPE Trans.* **1964**, *4*, 315–362.

18 J. D. Hoffman, R. L. Miller, *Macromolecules* **1988**, *21*, 3038–3051.

19 J. D. Hoffman, *Polymer* **1991**, *32*, 2828–2841.

20 H. L. Chen, H. H. Liu, J. S. Lin, *Macromolecules* **2000**, *33*, 4856–4860.

21 J. Liu, B. J. Jungnickel, *J. Phys. Chem. B* **2007**, *111*, 1917–1931.

22 L. Zhao, X. Peng, X. Liu, Y. Wang, S. Qin, J. Zhang, *Polym. J.* **2013**, *45*, 929–937.

23 W.-C. Lai, W.-B. Liau, T.-T. Lin, *Polymer* **2004**, *45*, 3073–3080.

24 M. Sheth, R. A. Kumar, V. Dave, R. A. Gross, S. P. Mccarthy, *J. Appl. Polym. Sci.* **1997**, *66*, 1495–1505.

25 P.-C. Kuo, C.-T. Lo, C.-Y. Chen, *Polymer* **2013**, *54*, 6654–6662.

26 L. Finelli, N. Lotti, A. Munari, *Eur. Polym. J.* **2002**, *38*, 1987–1993.

27 A. Alksnis, D. Deme, *J. Polym. Sci. Polym. Chem. Ed.* **1979**, *17*, 2701–2706.

28 A. Ballistreri, D. Garozzo, M. Giuffrida, G. Impallomeni, G. Montaudo, *Polym. Degrad. Stabil.* **1988**, *21*, 311–321.

29 G. R. Strobl, M. Schneider, *J. Polym. Sci. Polym. Phys. Ed.* **1980**, *18*, 1343–1359.

30 R. K. Verma, V. Velikov, R. G. Kander, H. Marand, B. Chu, B. S. Hsiao, *Polymer* **1996**, *37*, 5357–5365.

31 W. Ruland, *J. Appl. Crystallogr.* **1971**, *4*, 70–73.

32 P. Debye, A. M. Bueche, *J. Appl. Phys.* **1949**, *20*, 518–525.

33 A. J. Lovinger, D. D. Davis, F. J. Padden, *Polymer* **1985**, *26*, 1595–1604.

34 J. S. Chung, P. Cebe, *Polymer* **1992**, *33*, 2312–2324.

35 P. Cebe, S. D. Hong, *Polymer* **1986**, *27*, 1183–1192.

36 J. D. Hoffman, J. J. Weeks, *J. Res. Natl. Bur. Stand.* **1962**, *A66*, 13.

37 E. Meaurio, E. Zuza, J. R. Sarasua, *Macromolecules* **2005**, *38*, 1207–1215.

38 W. C. Lai, W. B. Liau, T. T. Lin, *Polymer* **2004**, *45*, 3073–3080.

39 C. I. Huang, S. H. Tsai, C. M. Chen, *J. Polym. Sci. Part B: Polym. Phys.* **2006**, *44*, 2438–2448.

40 B. S. Hsiao, Z. G. Wang, F. Yeh, Y. Gao, K. C. Sheth, *Polymer* **1999**, *40*, 3515–3523.

41 Z. G. Wang, B. S. Hsiao, B. X. Fu, L. Liu, F. Yeh, B. B. Sauer, H. Chang, J. M. Schultz, *Polymer* **2000**, *41*, 1791–1797.

42 H. Hama, H. K. Tashiro, *Polymer* **2003**, *4*, 2159–2168.

43 H. D. Keith, F. J. Padden, T. P. Russell, *Macromolecules* **1989**, *22*, 666–675.

44 Y. Wang, J. F. Mano, *J. Appl. Polym. Sci.* **2007**, *105*, 3500–3404.

45 F. B. Khambatta, F. Warner, T. P. Russell, R. S. Stein, *J. Polym. Sci. Polym. Phys. Ed.* **1976**, *14*, 1391–1424.

46 J. M. Yang, H. L. Chen, J. W. You, J. C. Hwang, *Polym. J.* **1997**, *29*, 657–662.

47 H. Xiao, W. Lu, J. T. Yeh, *J. Appl. Polym. Sci.* **2009**, *113*, 112–121.

48 J. I. Lauritzen, J. D. Hoffman, *J. Appl. Phys.* **1973**, *44*, 4340–4352.

49 R. Vasanthakumari, A. J. Pennings, *Polymer* **1983**, *24*, 175–178.

50 T. T. Wang, T. Nishi, *Macromolecules* **1977**, *10*, 421–425.

51 M. L. Di Lorenzo, *Polymer* **2001**, *42*, 9441–9446.

52 H. Tsuji, Y. Tezuka, S. K. Saha, M. Suzuki, S. Itsuno, *Polymer* **2005**, *46*, 4917–4927.

53 H. Tsuji, H. Takai, S. K. Saha, *Polymer* **2006**, *47*, 3826–3837.

54 Y. He, Z. Fan, Y. Hu, T. Wu, J. Wei, S. Li, *Eur. Polym. J.* **2007**, *43*, 4431–4439.

55 G. Strobl, T. Y. Cho, *Eur. Phys. J. E* **2007**, *23*, 55–65.

56 G. Strobl, *Rev. Mod. Phys.* **2009**, *81*, 1287–1300.

57 J. D. Hoffman, G. T. Davis, J. I. Lauritzen, *Treatise Solid State Chem.* **1976**, *3*, 497–614.